Kepler-539: A young extrasolar system with two giant planets on wide orbits and in gravitational interaction

(Article begins on next page)

26 June 2024

Kepler-539: a young extrasolar system with two giant planets on wide orbits and in gravitational interaction

L. Mancini[1,2], J. Lillo-Box[3,4], J. Southworth[5], L. Borsato[6],
D. Gandolfi[7,8], S. Ciceri[1], D. Barrado[3], R. Brahm[9,10], and Th. Henning[1]

[1] Max Planck Institute for Astronomy, Königstuhl 17, 69117 – Heidelberg, Germany
   e-mail: mancini@mpia.de
[2] INAF – Osservatorio Astrofisico di Torino, via Osservatorio 20, 10025 – Pino Torinese, Italy
[3] Depto. de Astrofísica, Centro de Astrobiologìa (CSIC-INTA), ESAC campus 28691 – Villanueva de la Cañada, Spain
[4] European Southern Observatory, Alonso de Cordova 3107, Vitacura, Casilla 19001, Santiago de Chile, Chile
[5] Astrophysics Group, Keele University, Keele ST5 5BG, UK
[6] Dip. di Fisica e Astronomia "Galileo Galilei", Università di Padova, Vicolo dell'Osservatorio 2, 35122 – Padova, Italy
[7] Dip. di Fisica, Università di Torino, via P. Giuria 1, 10125 – Torino, Italy
[8] Landessternwarte Königstuhl, Zentrum für Astronomie der Universität Heidelberg, Königstuhl 12, 69117 – Heidelberg, Germany
[9] Instituto de Astrofísica, Pontificia Universidad Católica de Chile, Av. Vicuña Mackenna 4860, 7820436 – Macul, Santiago, Chile
[10] Millennium Institute of Astrophysics, Av. Vicuña Mackenna 4860, 7820436 – Macul, Santiago, Chile

Preprint online version: April 22, 2016

ABSTRACT

We confirm the planetary nature of Kepler-539 b (aka Kepler object of interest K00372.01), a giant transiting exoplanet orbiting a solar-analogue G2 V star. The mass of Kepler-539 b was accurately derived thanks to a series of precise radial velocity measurements obtained with the CAFE spectrograph mounted on the CAHA 2.2-m telescope. A simultaneous fit of the radial-velocity data and *Kepler* photometry revealed that Kepler-539 b is a dense Jupiter-like planet with a mass of $M_\mathrm{p} = 0.97 \pm 0.29\,M_\mathrm{Jup}$ and a radius of $R_\mathrm{p} = 0.747 \pm 0.018\,R_\mathrm{Jup}$, making a complete circular revolution around its parent star in 125.6 days. The semi-major axis of the orbit is roughly 0.5 au, implying that the planet is at ≈ 0.45 au from the habitable zone. By analysing the mid-transit times of the 12 transit events of Kepler-539 b recorded by the *Kepler* spacecraft, we found a clear modulated transit time variation (TTV), which is attributable to the presence of a planet c in a wider orbit. The few timings available do not allow us to precisely estimate the properties of Kepler-539 c and our analysis suggests that it has a mass between 1.2 and $3.6\,M_\mathrm{Jup}$, revolving on a very eccentric orbit $(0.4 < e \le 0.6)$ with a period larger than 1000 days. The high eccentricity of planet c is the probable cause of the TTV modulation of planet b. The analysis of the CAFE spectra revealed a relatively high photospheric lithium content, $A(\mathrm{Li}) = 2.48 \pm 0.12$ dex, which, together with both a gyrochronological and isochronal analysis, suggests that the parent star is relatively young.

Key words. stars: planetary systems – stars: fundamental parameters – stars: individual: Kepler-539

1. Introduction

The transiting extrasolar planet (TEP) population turns out to be the best *atout* in the hands of exoplanetary scientists. Thanks to the early ground-based systematic surveys (e.g., Bakos et al. 2004; Alonso et al. 2004; McCullough et al. 2005; Pollacco et al. 2006; Pepper et al. 2007; Alsubai et al. 2013; Bakos et al. 2013) and then to those from the space (CoRoT: Barge et al. 2008, *Kepler*: Borucki et al. 2011), more than 1290 transiting planetary systems have now been found. The possibility to easily derive most of their physical and orbital parameters, and to investigate even the composition of their atmosphere, make the TEPs the most suitable targets to detect and study in detail. They currently represent the best statistical sample to constrain the theoretical models of planetary formation and evolution. Moreover, transit time variation (TTV) studies allowed the detection of additional non-transiting bodies in many TEP systems, highlighting the great efficacy of high-precision and high-cadence photometry in the search for extrasolar planets.

The majority of TEPs have been discovered by the *Kepler* space telescope, which has revealed how varied they are, in terms of mass and size, and how diverse their architectures can be, confirming science-fiction pictures in several cases or going beyond human imagination in others. The numerous TEP discoveries achieved by *Kepler* are based on time-series photometric monitoring of the brightness of over 145 000 main sequence stars, in which the periodic-dimming signal caused by a TEP can be found. However, such a signal can be mimic by other astrophysical objects in particular configurations. Radial velocity (RV) follow-up observations of the 'potential' parent stars are therefore a fundamental step for distinguishing real TEPs from false positive cases.

Here we focus our attention on the *Kepler* system Kepler-539. Thanks to precise RV measurements, presented

in Sect. 2, we confirm the planetary nature of Kepler-539 b (aka KOI-372 b, K00372.01, KIC 6471021), a dense gas-giant planet moving on a wide orbit around a young and active G2 V star ($V = 12.6$ mag). The analysis of the physical parameters of Kepler-539 b and its parent star are described in Sect. 3. Moreover, the clear variation observed in the mid-times transits of Kepler-539 b strongly support the existence of an additional massive planet, Kepler-539 c, in the system, moving on a larger and very eccentric orbit, as discussed in Sect. 4. We summarise our results in Sect. 5.

2. Observations and data analysis

2.1. Kepler photometry

The *Kepler* spacecraft monitored Kepler-539 from quarters 0 to 17 (i.e. four years; from May 2009 to May 2013). It was labelled as a *Kepler* object of interest (KOI) due to a $\sim 0.2\%$ dimming in its light curve with a period of ~ 125 days (Borucki et al. 2011). This periodic dimming is actually caused by the transit of a Jupiter-like planet candidate, Kepler-539 b, moving on a quite wide orbit around the star. 12 transits of Kepler-539 b are present in the *Kepler* long cadence (LC) light curves. We have labelled them from cycle -5 to cycle 6 (see Fig. 1). Two of the transits are incomplete (cycles -2 and -1); two are most likely contaminated by starspot crossing anomalies (cycles -5 and 2); three were also covered in short cadence (SC) (cycles 4, 5 and 6; see Fig. 2). The complete *Kepler* light curve is shown in Fig. 3, which highlights a significant stellar variability (0.0470 ± 0.0002 mag peak-to-peak). McQuillan et al. (2013) found a periodic photometric modulation in the light curve and, by assuming that it is induced by a star-spot activity, estimated a stellar rotation period of 11.769 ± 0.016 days. This value is in good agreement with that found by Walkowicz & Basri (2013a,b), i.e. 11.90 ± 3.45 days.

2.2. Radial velocity follow-up observations

We monitored Kepler-539 between July 2012 and July 2015 with the Calar Alto Fibre-fed Echelle spectrograph (CAFE; Aceituno et al. 2013) mounted on the 2.2 m telescope at the Calar Alto Observatory (Almería, Spain) as part of our follow-up programme of *Kepler* candidates. This programme has already confirmed the planetary nature of Kepler-91 b (Lillo-Box et al. 2014a,b), Kepler-432 b (Ciceri et al. 2015), Kepler-447 b (Lillo-Box et al. 2015b), and has identified and characterised some false positives in the sample of *Kepler* planet candidates (Lillo-Box et al. 2015a). CAFE has a spectral coverage from 4000 Å to 9500 Å, divided into 84 orders with a mean resolving power of $R = 63\,000$. We acquired 28 spectra, which were reduced using the dedicated pipeline provided by the observatory (Aceituno et al. 2013). We used thorium-argon (ThAr) exposures obtained after each science spectrum to wavelength-calibrate the corresponding data. The final spectra have signal-to-noise ratios in the range S/N = 7–16. A radial velocity (RV) was obtained from each spectrum by using the cross-correlation technique through a weighted binary mask (Baranne et al. 1996). The mask is composed of more than 2000 sharp and isolated spectral lines in the CAFE wavelength range. The cross-correlation was performed in a ± 30 km s^{-1} range around the expected RV of the star. The peak of the cross-correlation function (CCF) was measured by fitting a four-term Gaussian profile. This velocity was then corrected for the barycentric Earth radial velocity at mid-exposure time. Since we took several consecutive spectra on the same nights, we decided to combine the RV values of the corresponding pairs in the cases where their individual signal-to-noise was low (i.e., S/N < 10) and mutual discrepancies were larger than 50 m s^{-1}. This procedure can also diminish the effect of short term variability, such as the granulation noise, on the radial velocity (although here the expected amplitudes are of the order of few tens of m s^{-1}). Some of the spectra were neglected due to low quality, mainly caused by weather conditions or problems with the stability of the ThAr lamp. We obtained 20 RV values in total which are reported, together with their observing times, in Table 1 and are compatible with the presence of a $\sim 1 \, M_{\mathrm{Jup}}$ planet in the system (see Fig. 7 and Sect. 4).

Table 1: RV and BVS measurements of Kepler-539 from CAHA/CAFE.

Date of observation BJD(TDB)-2450000	RV (km s^{-1})	err$_{\mathrm{RV}}$ (km s^{-1})	FWHM (km s^{-1})	BVS (km s^{-1})
6116.5291378	10.408	0.026	-0.041	9.696
6124.3823828	10.383	0.029	-0.065	9.517
6138.4327769	10.387	0.018	-0.117	9.656
6523.4275256	10.402	0.024	-0.100	9.572
6598.2879800	10.448	0.033	0.081	9.518
6804.5209537	10.439	0.029	-0.146	9.250
6811.4391381	10.475	0.035	0.159	9.407
6821.6225006	10.432	0.049	-0.118	9.198
6834.4194255	10.437	0.025	0.086	9.342
6859.5818459	10.409	0.038	-0.391	10.036
7136.6259467	10.285	0.039	-0.266	9.541
7152.5198831	10.431	0.042	0.087	9.422
7160.5096750	10.450	0.021	-0.267	9.312
7169.5836757	10.500	0.032	0.038	9.153
7193.4502198	10.425	0.045	-0.088	9.556
7254.4473639	10.361	0.035	-0.021	9.727
7258.3855966	10.400	0.045	-0.106	9.559
7263.4322174	10.402	0.028	0.014	9.519
7264.4220946	10.413	0.025	0.018	9.599
7266.3737337	10.449	0.034	0.169	9.995

2.3. Spectral analysis and the age of Kepler-539

We derived the spectroscopic parameters of the host star Kepler-539 from the co-added CAFE spectra, which has a S/N ratio of about 40 per pixel at 5500 Å. Following the procedures described in Gandolfi et al. (2013, 2015), we used a customised IDL[1] software suite to fit the composite CAFE spectrum to a grid of synthetic theoretical spectra. The latter were calculated with the stellar spectral synthesis program SPECTRUM (Gray & Corbally 1994) using ATLAS9 plane-parallel model atmospheres (Kurucz 1979), under the assumptions of local thermodynamic equilibrium (LTE) and solar atomic abundances as given in Grevesse & Sauval (1998). We fitted spectral features that are sensitive to different photospheric parameters. Briefly, we used the wings of the Balmer lines to estimate the effective temperature T_{eff} of the star, and the Mg I 5167, 5173, and 5184 Å,

---

[1] The acronym IDL stands for Interactive Data Language and is a trademark of ITT Visual Information Solutions.
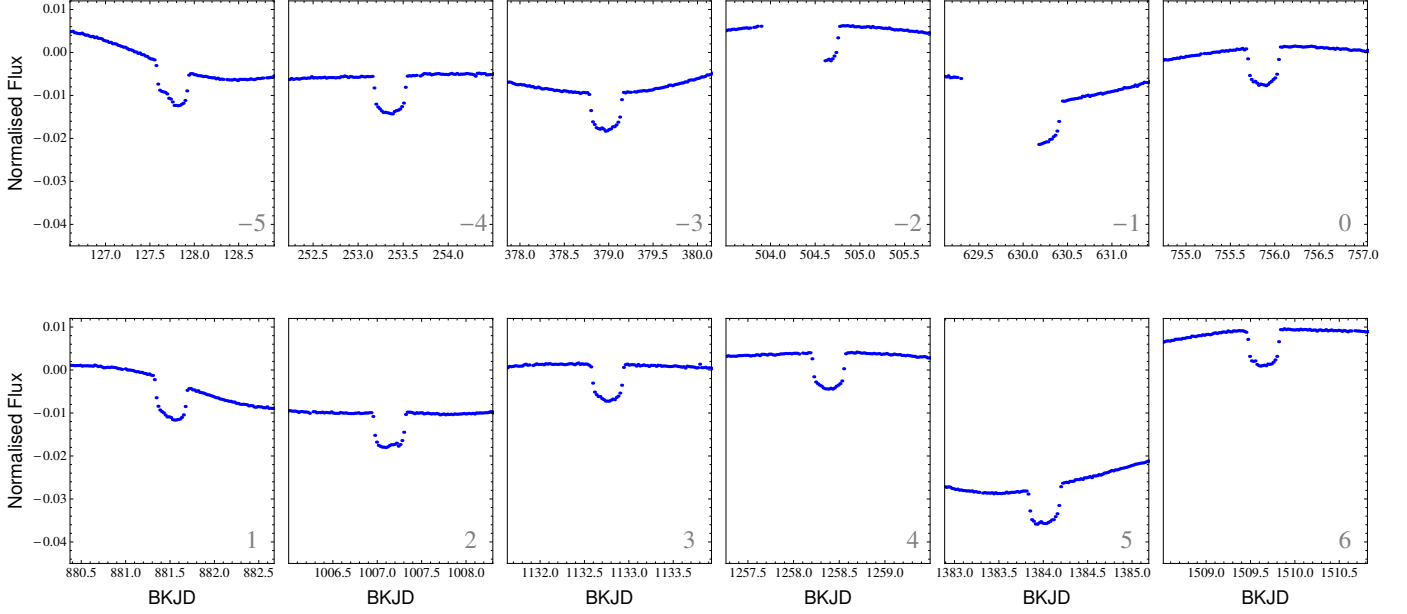
Fig. 1: The twelve transit events of Kepler-539 b observed by *Kepler* in long-cadence mode. The transits at epoch -5 and 2 are clearly affected by star-spot-crossing events. Times are in BKJD (Barycentric Kepler Julian Date – equivalent to BJD(TDB) minus 2454833.0).
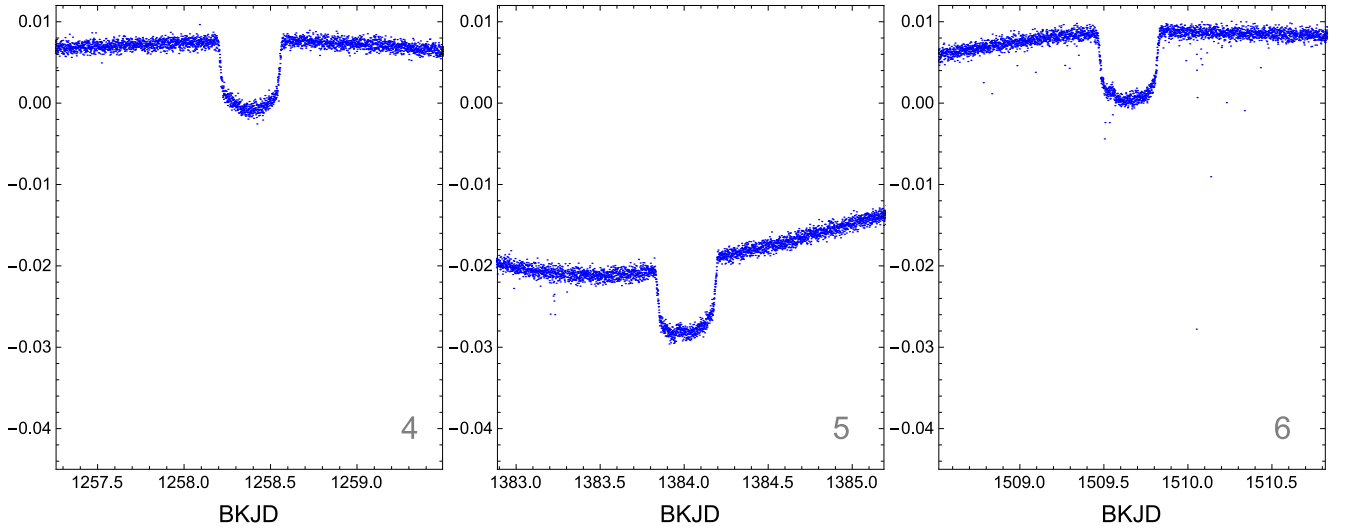

Fig. 2: The three transit events of Kepler-539 b observed by *Kepler* in short-cadence mode. Times are in BKJD (Barycentric Kepler Julian Date – equivalent to BJD(TDB) minus 2454833.0).

the Ca I 6162 and 6439 Å, and the Na I D lines to determine the surface gravity $\log g_\star$. The iron abundance [Fe/H] and microturbulent velocity v_{micro} was derived by applying the method described in Blackwell & Shallis (1979) on isolated Fe I and Fe II lines. To determine the macroturbulent velocity v_{macro}, we adopted the calibration equations for solar like stars from Doyle et al. (2014). The projected rotational velocity $v \sin i_\star$ was measured by fitting the profile of several clean and unblended metal lines[2]. We found that Kepler-539 has an effective temperature of $T_{eff} = 5820 \pm 80$ K, $\log g_\star = 4.4 \pm 0.1$ (cgs), [Fe/H]$= -0.01 \pm 0.07$ dex, $v_{micro} = 1.1 \pm 0.1$ km s^{-1}, $v_{macro} = 3.2 \pm 0.6$ km s^{-1}, and

_____

[2] Here $i_\star$ refers to the inclination of the stellar rotation axis with respect to the line of sight.
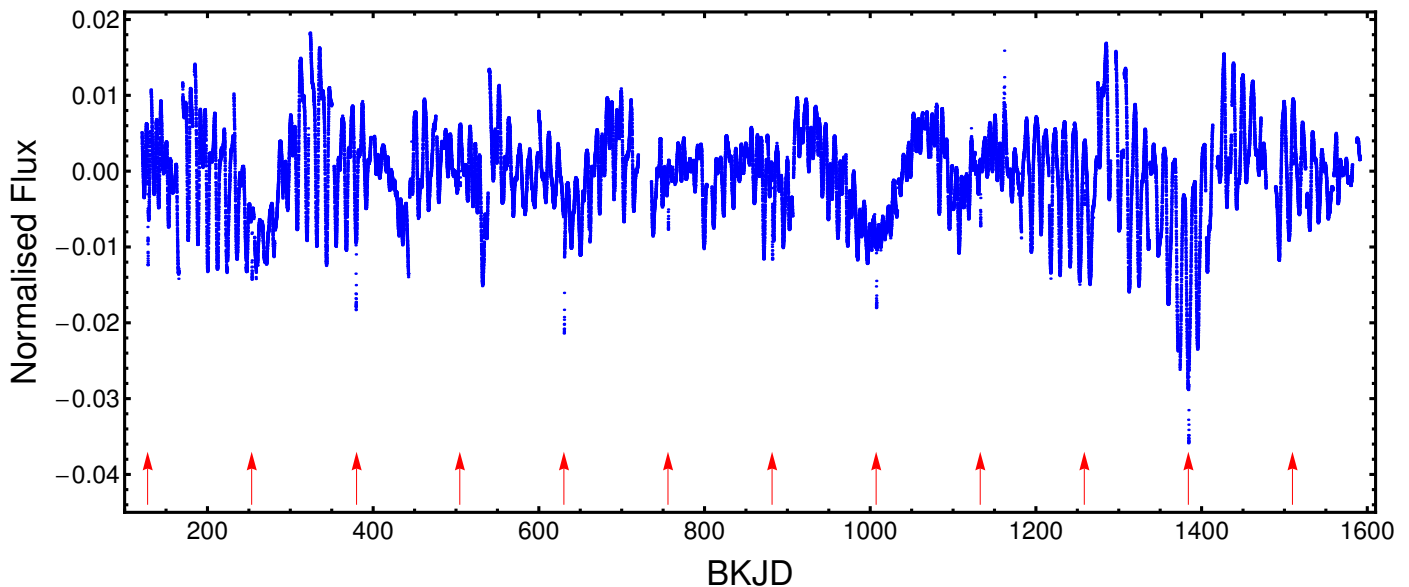
Fig. 3: The entire *Kepler* light-curve data of Kepler-539. The large stellar variability can be reasonable interpreted as induced by a star-spot activity. Times are in BKJD (Barycentric Kepler Julian Date – equivalent to BJD(TDB) minus 2454833.0). The red arrows mark the mid-times of the twelve transits of Kepler-539 b.

$v \sin i_\star = 4.4 \pm 0.5 \text{ km s}^{-1}$ (Table 3). According to the Straizys & Kuriliene (1981) calibration scale for dwarf stars, the effective temperature of Kepler-539 translates to a G2 V spectral type.
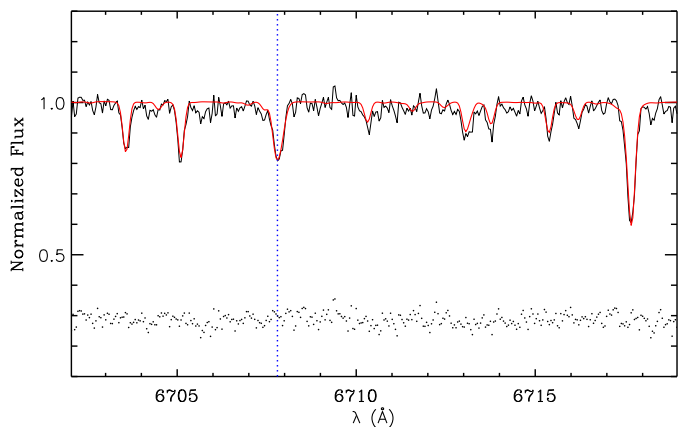

Fig. 4: CAFE co-added spectrum of Kepler-539 (black line) encompassing the Li I 6707.8 Å absorption doublet. The best fitting ATLAS9 spectrum is overplotted with a thick red line. The vertical dashed line marks the position of the Li doublet. The lowest part of the plot displays the residuals to the fit.

The CAFE co-added spectrum of Kepler-539 reveals the presence of a moderate Li I 6707.8 Å absorption doublet (Fig. 4). We estimated the photospheric lithium abundance of the star by fitting the Li doublet using ATLAS9 LTE model atmospheres. We fixed the stellar parameters to the values given in Table 3 and allowed our code to fit the lithium content. Adopting a correction for non-LTE

effects of $+0.006$ dex (Lind et al. 2009), we measured a lithium abundance of $A(\text{Li}) = \log(n(\text{Li})/n(\text{H})) + 12 = 2.48 \pm 0.12$ dex.

The photospheric lithium content and the moderate rotation period of Kepler-539 suggest that the star is relatively young. Fig. 5 shows the lithium abundance of Kepler-539 compared to the $A(\text{Li})$ of the dwarf stars of the Pleiades, Hyades, and NGC 752 open clusters, as listed in Soderblom et al. (1993), Pace et al. (2012), and Sestito et al. (2004), respectively. Kepler-539 has to be older than ~ 0.1 Gyr, as the star falls below the envelope of the Pleiades. Although lithium depletion becomes ineffective beyond an age of 1–2 Gyr (Sestito & Randich 2005), Kepler-539 lies between the envelopes of the other two clusters, suggesting an age intermediate between the age of the Hyades (~ 0.6 Gyr) and the age of NGC 752 (~ 2.0 Gyr). This is further confirmed by the fact that the lithium content of Kepler-539 is intermediate between the average lithium abundance measured in early G-type stars of 0.6-Gyr-old open clusters ($A(\text{Li}) = 2.58 \pm 0.15$ dex) and that of 2-Gyr-old open clusters ($A(\text{Li}) = 2.33 \pm 0.17$ dex; Sestito & Randich 2005).

We used Eq. (32) from Barnes (2010) and the rotation period of Kepler-539 to infer its gyrochronological age, assuming a convective turnover time-scale of $\tau_c = 34$ days (Barnes & Kim 2010) and a zero-age main sequence rotation period of $P_0 = 1.1$ days (Barnes 2010). We found a gyrochronological age of 1.0 ± 0.3 Gyr, which supports the relatively young scenario. Our estimation is in good agreement with the 1.15 Gyr gyrochronological age predicted by Walkowicz & Basri (2013a,b) and with that estimated using theoretical models (see Sect. 3 and Table 3).

By having short-cadence data over a quite large timespan, it is in principle possible to perform an asteroseismic analysis and try to precisely estimate the age of a star. However, in the case of Kepler-539, the SC data are only available for less than half the quarters. In particular, the

continuous time baseline of SC data is not more than 125 d in the best case (BJD 2456015 − 2456139). Furthermore the activity variation is predominant in the data. We analysed such SC data by filtering the variability due to activity with moving averages, but we did not find evidence of a clear frequency comb in the power spectrum and therefore we did not get particular clues about patterns due to solar-like oscillations. We concluded that no reliable asteroseismic analysis could be performed for Kepler-539 based on the *Kepler* data.
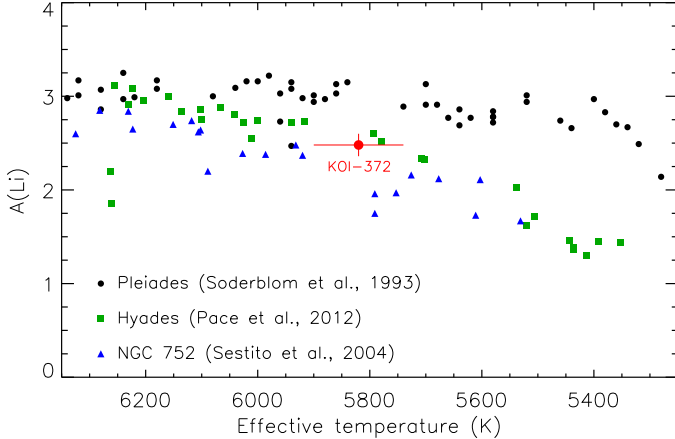

Fig. 5: Lithium abundances of F- and G-type dwarf stars in the Pleiades (black dots; Soderblom et al. 1993), Hyades (green squares; Pace et al. 2012), and NGC 752 (blue triangles; Sestito et al. 2004) open clusters. The red dot marks the position of Kepler-539.

2.4. Excluding false-positive scenarios

A faint pulsating variable star or a binary system in the background/foreground can mimic a planetary transit signal on the target star. High-resolution images are extremely useful to exclude this possibility (e.g., Lillo-Box et al. 2014c). A K_s-band, high-resolution, adaptive optics image of Kepler-539 was obtained with ARIES on the 6.5 m MMT telescope by Adams et al. (2012), who found four stars within 6″ of the target, see Table 2. Following Lillo-Box et al. (2012), we have estimated the dilution effect caused by each companion, finding that it is very small for the three closest targets, roughly 0.023% in total and thus negligible. Concerning the very bright companion "E", this is another object targeted as KIC 6471028. As it lies outside the *Kepler* aperture, this star does not contaminate Kepler-539. KIC 6471028 was also detected with the AstraLux North instrument mounted on the CAHA 2.2 m telescope by Lillo-Box et al. (2012), who estimated that this is a K2-K4 background dwarf.

An intense stellar activity could mimic the presence of a planetary body in the RV signal, thus causing a false positive case. We have also analysed such a possibility by determining the bisector velocity span (BVS) from the CAFE spectra (the values are reported in Table 1). The bisector analysis provides a Pearson correlation coefficient between the RV and the BVS of $0.28^{+0.31}_{-0.42}$ (median value and 95% confidence intervals from the posterior probability distri-

Table 2: Nearby visual companions around Kepler-539 (from Adams et al. 2012) and their dilution effect on the depth of the transit events.

Companion	Distance (″)	K_s (mag)	ΔK_s	Dilution
B	2.49	23.2	8.6	0.005 %
C	3.56	22.4	8.0	0.01 %
D	4.99	22.7	8.2	0.008 %
E[a]	5.94	17.1	4.0	1.31 %

Notes. [a] Also known as KIC 6471028.

bution, see Figueira et al. 2016). This value indicates only a weak correlation between the two parameters, which is only significant at a 2σ level for the median value and still at less than 3σ for the upper boundary. Consequently, we assume no correlation between both parameters, although we warn about the weak probability of correlation.
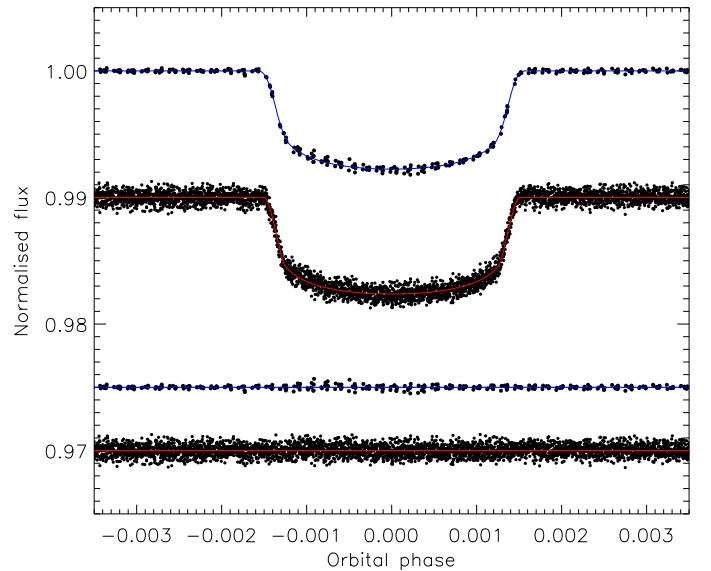
3. Physical properties of the system

Fig. 6: Phased Kepler long-cadence (top light curve) and short-cadence (bottom light curve) data zoomed around transit phase. The TTVs (see Sect. 4) were removed from the data before plotting. The JKTEBOP best fits are shown using solid lines. The residuals of the fits are plotted at the base of the figure.

For the determination of the physical parameters of the Kepler-539 system, we proceeded as in Ciceri et al. (2015). We first selected for analysis all data within two transit durations of a transit, ignoring the two with only partial coverage in the *Kepler* light curve, and converted from flux to magnitude units. Each transit was then detrended by fitting a polynomial versus time. High polynomial orders of 3 to 5 were required to account for the brightness variations of the host star caused by spot activity.

We then fitted the photometry and the CAFE RV measurements simultaneously using the JKTEBOP code (Southworth 2013), after modifying it to allow fitting for individual times of mid-transit. The *Kepler* LC and SC

5

Table 3: Final parameters of the planetary system KOI-0372.

Parameter	Nomen.	Unit	Value[a]
Stellar parameters			
R.A. (J2000)	....	....	$19^{\mathrm{h}}56^{\mathrm{m}}29{:}39^{\mathrm{s}}$
Dec. (J2000)	....	....	$41°52'00.3''$
Spectral type[b]	....	....	G2 V
Kepler magnitude	...... K_{p}	.....mag	12.39
Effective temperature	...... T_{eff}	......K	5820 ± 80
Iron abundance	.... [Fe/H]	.....dex	-0.01 ± 0.07
Lithium abundance	..... $A(\mathrm{Li})$	.....dex	2.5 ± 0.1
Microturb. velocity	..... v_{micro}	... km s^{-1} ...	1.1 ± 0.1
Macroturb. velocity[c]	.... v_{macro}	... km s^{-1} ...	3.2 ± 0.6
Proj. rotat. velocity	.... $v \sin i_\star$	... km s^{-1} ...	4.4 ± 0.5
Stellar rotation period[d]	...... P_{rot}	.....day	11.769 ± 0.016
Stellar age (from gyrochronology) .	....	.....Gyr	1.0 ± 0.3
Stellar age (from isochrones)	....	.....Gyr	$1.1^{+0.6\,+0.3}_{-0.0\,-0.1}$
Stellar mass	...... $M_\star$	..... $M_\odot$	$1.048 \pm 0.034 \pm 0.025$
Stellar radius	...... $R_\star$	..... $R_\odot$	$0.952 \pm 0.017 \pm 0.007$
Stellar mean density	...... $\rho_\star$	..... $\rho_\odot$	1.216 ± 0.054
Stellar surface gravity	..... $\log g_\star$	.....cgs	$4.502 \pm 0.014 \pm 0.003$
Planetary parameters (Kepler-539 b)			
Planetary mass	...... M_{b}	.... M_{Jup}	$0.97 \pm 0.29 \pm 0.02$
Planetary radius	...... R_{b}	.... R_{Jup}	$0.747 \pm 0.016 \pm 0.006$
Planetary mean density	...... ρ_{b}	..... ρ_{Jup}	$2.18 \pm 0.66 \pm 0.02$
Planetary surface gravity	...... g_{b}	.... m s^{-2}	43 ± 12
Planetary equilibrium temperature	...... T_{eq}	......K	387.6 ± 6.0
Safronov number	...... Θ	....	$1.24 \pm 0.37 \pm 0.01$
Orbital parameters			
Time of mid-transit	...... T_0	.. BJD$_{\mathrm{TDB}}$ ..	$2\,455\,588.8710 \pm 0.0030$
Orbital period	..... P_{orb}	.... days	125.63243 ± 0.00071
Semi-major axis	.... a	..... au	$0.4988 \pm 0.0054 \pm 0.0039$
Orbital inclination	.... i	....degree	89.845 ± 0.086
Fractional star radius	...... r_{A}	....	0.01057 ± 0.00078
Fractional planet radius	...... r_{b}	....	0.000854 ± 0.000085
RV semi-amplitude	...... K_{A}	.... m s^{-1}	132.3 ± 6.3
Barycentric RV	...... γ	... km s^{-1} ...	9.959 ± 0.007
Eccentricity	.... e	....	$< 0.39^{e}$

Notes. Where there are two error bars, the first is a statistical error, coming from the measured spectroscopic and photometric parameters, while the second is a systematic error and is given only for those parameters which have a dependence on theoretical stellar models.
[a] The adopted parameters assume a circular orbit.
[b] With an accuracy of ± 1 sub-class.
[c] Using the calibration equations of Doyle et al. (2014).
[d] From McQuillan et al. (2013).
[e] The 99% confidence upper limit on the eccentricity from a model in which the eccentricity is allowed to vary in the fit.

data were fitted separately, accounting for the long effective exposure times in the LC data by oversampling the fitted model by a factor of five.

The following parameters were fitted: the fractional radii of the two objects ($r_\star = R_\star/a$ and $r_{\mathrm{p}} = R_{\mathrm{p}}/a$, where a is the orbital semi-major axis), the orbital inclination i, the time of midpoint of each transit, the velocity amplitude $K_\star$, the systemic velocity V_γ, and the coefficients of the polynomial for each transit. The orbital period, P_{orb}, and reference transit midpoint, T_0, were fixed to the values measured from the transit times; these were used only for phasing the RV measurements. As in the other papers of our series (e.g. Mancini et al. 2013a,b), a quadratic limb darkening law was used, with the linear term fitted and the

quadratic term fixed to 0.27 (Sing 2010). We rescaled the error bars of the LC, SC and RV data to give a reduced χ^2 of $\chi^2_\nu = 1.0$ for each versus the fitted model. Based on our experience with similar studies (e.g. Mancini et al. 2014a,b), this procedure is necessary for taking into account underestimated data errors and additional sources of white noise; for example an RV jitter due to the activity of the host star.

The best fits to the photometry and the RVs are shown in Figs. 6 and 7. The uncertainties in the fitted parameters were derived by running both Monte Carlo and residual-permutation simulations (Southworth 2008) and choosing the larger of the two error bars for each parameter. The results obtained using the SC data are more precise than
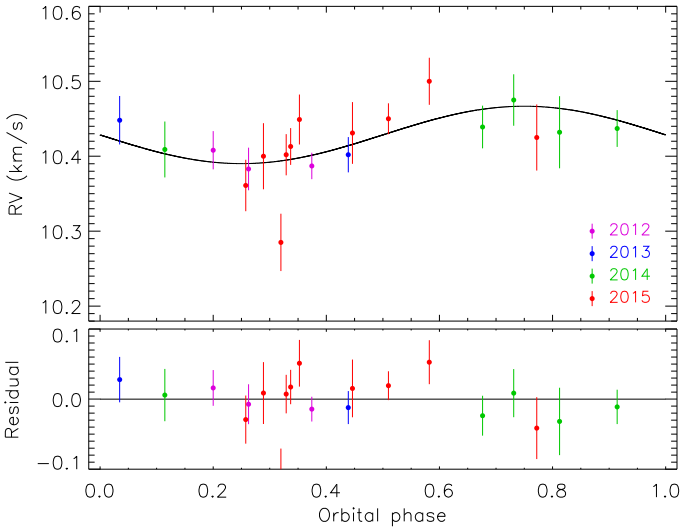
Fig. 7: Upper panel: phased RVs for Kepler-539 and the best fit from JKTEBOP. Lower panel: residuals of RVs versus best fit.

those from the LC data, so were adopted as the final set of photometric parameters.

We find that the observations are fully consistent with Kepler-539 b moving on a circular orbit. However, we performed the fit both fixing the orbital eccentricity e to zero and fitting for it via the combination terms $e \cos \omega$ and $e \sin \omega$, where ω is the argument of periastron. In the latter case, we obtained $e = 0.18^{+0.21}_{-0.18}$. We then used the Bayesian information criterion (BIC) to evaluate the preferred scenario, finding that the eccentric case is not favoured over the zero eccentricity model.

Finally, we estimated the age and the physical properties of the system from the SC results and the $T_{\rm eff}$ and [Fe/H] measured from our spectra. Constraints from theoretical stellar models were used to make the solution determinate. We followed the HSTEP approach (Southworth 2012, and references therein), which yielded measurements of the properties of the star and planet accompanied by both statistical and systematic errorbars. The final results are reported in Table 3.

4. Planet Kepler-539 c from transit time variation

We have analysed the 12 mid-transit times of Kepler-539 b to characterise the ephemeris of the transit and check if there is a possible transit time variation (TTV), which could be a sign of the presence of additional bodies in this system. Since the transits at cycles -5 and 2 are quite affected by starspots, we used the PRISM[3] and GEMC[4] codes (Tregloan-Reed et al. 2013, 2015) that allowed us to fit both the full transit events and the shorter starspot-occultation events contemporaneously. The parameters of the starspots coming from the fits are reported in Appendix A. The mid-transit times for the other epochs were estimated using JK-TEBOP. The resulting timings are tabulated in Table 4 and were fitted with a straight line to obtain the orbital period, $P_{\rm orb} = 125.63243 \pm 0.00071$ days, and the reference time

[3] Planetary Retrospective Integrated Star-spot Model.
[4] Genetic Evolution Markov Chain.

Table 4: *Kepler* times of transit midpoint of Kepler-539 b and their residuals.

Time of minimum BJD(TDB)−2400000	Cycle no.	Residual (JD)
54960.74947 ± 0.00109	-5	0.040612
55086.35000 ± 0.00040	-4	0.008712
55212.96694 ± 0.00042	-3	-0.006781
55337.57977 ± 0.00043	-2	-0.026380
55463.23346 ± 0.00118	-1	-0.005126
55588.87808 ± 0.00041	0	0.007068
55714.51794 ± 0.00043	1	0.014495
55840.13340 ± 0.00096	2	-0.002478
55965.77212 ± 0.00043	3	0.003803
56091.39778 ± 0.00030	4	-0.002963
56217.00030 ± 0.00030	5	-0.001233
56342.66701 ± 0.00030	6	0.001403

Table 5: The next mid-transit times of Kepler-539 b.

Cycle	BJD(TDB)	Date		Time (UT)
16	2457598.9899	2016 Jul	29	11:40
17	2457724.6223	2016 Dec	02	02:56
18	2457850.2547	2017 Apr	06	18:07
19	2457975.8872	2017 Aug	10	09:12
20	2458101.5196	2017 Dec	14	00:29

of mid-transit, $T_0 = 2\,455\,588.8710 \pm 0.0030$ BJD (TDB). A plot of the residuals around the fit (see Fig. 8) shows a clear and modulated deviation from the predicted transit times, meaning that the orbital period of Kepler-539 b is variable (the maximum TTV is 58.5 ± 1.6 min and was measured for the transit at cycle −5). The uncertainties of $P_{\rm orb}$ and T_0 have been increased to account for this, but we stress that these values should be used with caution as they are based on only 12 timings, of which two are incomplete and others are affected by starspot anomalies that can introduce offsets in the transit timing measurements – several studies have quantified this effect (e.g. Barros et al. 2013; Oshagh et al. 2013; Mazeh et al. 2015; Ioannidis et al. 2016). We have reported the predicted mid-transit times in Table 5 for the next year and a half.

In order to identify the origin of this modulated TTV, we used the TRADES (TRAnsits and Dynamics of Exoplanetary Systems; Borsato et al. 2014) code, which allows modelling of the dynamics of multiple-planet systems by reproducing the observed mid-transit times and RVs, with the possibility to choose among four different algorithms. We thus investigated the possibility that Kepler-539 is a planetary system formed by a star and two planets, b and c. We ran two series of simulations, the first by selecting the PIKAIA algorithm (Charbonneau 1995), the second with the Particle Swarm Optimization (PSO) algorithm (Tada 2007). In all the cases, we fixed tight boundaries for the parameters of planet **b** (centred on the values in Table 3) and assumed the zero eccentricity case, which means that we fixed the argument of pericentre ($\omega_{\rm b}$) to 90°, and let only the mean anomaly ($\nu_{\rm b}$) of planet b to freely float between 0 and 360 degrees. We use a time of reference (or epoch, $t_{\rm epoch} = 2455463.244$) that is very close to the transit cycle 0, forcing the planet b to be initially at the pericentre. Because of this, all the solutions of both the algorithms returned zero values for $\nu_{\rm b}$. Furthermore,
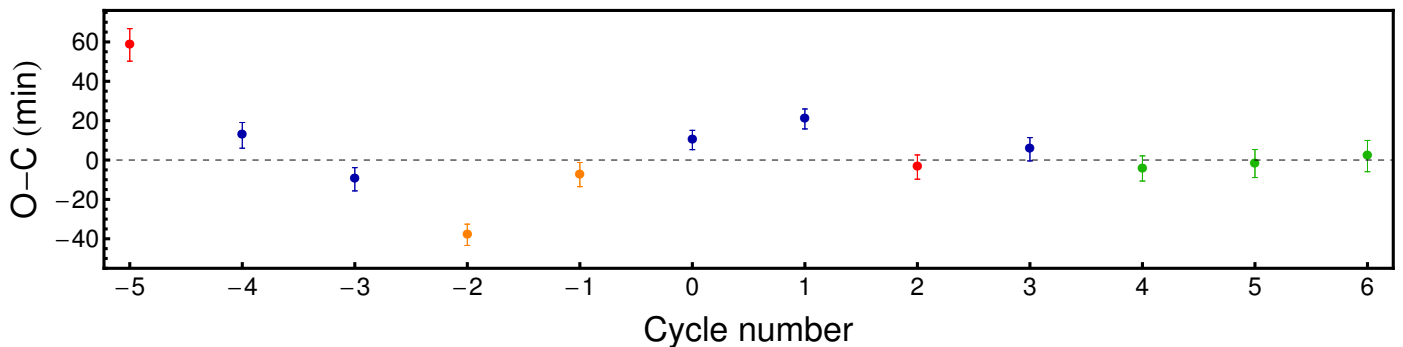
7

Fig. 8: O–C diagram for the timings of Kepler-539 b at mid-transit versus a linear ephemeris. The timings in blue refer to those coming from the *Kepler* LC data, while those marked with green are from SC data. The red points refer to the two LC transits affected by star spots. The two incomplete LC transits are marked with orange points.

we assumed for simplicity the two planets to be coplanar. We investigated different configurations of two planet system, with the period of planet c, P_c, varying from 150 to 2500 days. We fitted the pair $(e_c \cos \omega_c, e_c \sin \omega_c)$ instead of (e_c, ω_c) to avoid correlation between the parameters. We set 0.9 as the highest value allowed for the eccentricity, while we let ω_c and ν_c freely vary as for ν_b. The solutions obtained from the TRADES fitting processes were further analysed using the Frequency Map Analysis (FMA; Laskar et al. 1992) to check if they are stable.

We found that the best solutions are those related to configurations with $P_c > 1000$ days and a mass of the planet c between 1.2 and 3.6 $M_{\rm Jup}$ on a very eccentric orbit $(0.4 < e_c \le 0.6)$. The final parameters, with confidence intervals estimated with a bootstrapping method, are reported in Table 6 for the five best solutions, based on the χ^2, and displayed in figures shown in Appendix B. The estimated confidence intervals are very tight to the fitted values because the algorithms found solutions that correspond to minimum surrounded by very high peaks in the χ^2-space. We also exhaustively investigated narrow region $(200 - 800 \, {\rm days})$ of P_c (in steps of about 300 days), but the solutions that we obtained are not favoured because the corresponding χ^2 is much higher than those reported in Table 6.

Knowing the orbital period of Kepler-539 c, we can easily estimate the semi-major axis and the equilibrium temperature of the planet c for each solutions. These values are shown in right-hand columns of Table 6. Moreover, we can use Eq. (7.29) from Haswell (2010) for estimating the maximum TTV signal expected for Kepler-539 b, i.e.

$$\mathrm{TTV_{max}} = (M_A + M_b) e_c (a_b/a_c)^3 P_c. \tag{1}$$

The last column of Table 6 reports the values of $\mathrm{TTV_{max}}$ for each of the five solutions. The best TRADES solution is also that for which the maximum TTV signal is higher than the others and in better agreement with the observations.

Very interestingly, the high eccentricity of planet c gives a direct explanation of the modulation of the TTV of planet b: when planet c moves close to planet b, it gravitationally kicks its smaller sibling, causing the maximum in the TTV signal; after the conjunction, planet b re-circularizes own orbit very slowly, because of tidal interactions with the star and planet c moving far from it. This causes the decreasing of amplitude of its TTV that we see in Fig 8.

We again stress that all the values presented in Table 6 should be taken with caution, because the existence of

planet c can be definitively constrained only by new transit observations, able to completely cover the TTV phase of planet b. In particular, one should verify if there is a periodic repetition of the peak and the modulation.

5. Discussion and conclusions

Thanks to precise RV measurements obtained with the high-resolution spectrograph CAFE, we confirmed the planetary nature of Kepler-539 b, a dense Jupiter-like planet with a mass of $0.97 \pm 0.29 \, M_{\rm Jup}$ and a radius of $0.747 \pm 0.018 \, R_{\rm Jup}$, revolving with a period of 125.6 days on a circular orbit around a G2 V star, similar to the Sun. The parameters of the parent star and the planet b were obtained by analysing the CAFE spectra and through a joint fit to the RV data and *Kepler* transit light curves. Orbiting at ~ 0.5 au from its host, Kepler-539 b is located not so far $(\approx 0.45 \, {\rm au})$ from its *habitable zone* (HZ), which has a width of $\sim 0.72 \, {\rm au}$, as we estimated it based on the stellar parameters reported in Table 3 and the HZ calculator by Kopparapu et al. (2013, 2014). The parent star is quite active, as is shown by the 0.047 mag peak-to-peak modulation present in the long time-series photometry and from the star-spot anomalies clearly visible in two of the transit events monitored by *Kepler*. Even though it has physical characteristics that resemble those of the Sun, Kepler-539 is much younger: 1.0 ± 0.3 Gyr as estimated from its lithium abundance and gyrochronology.

An analysis of the *Kepler* mid-transit times of Kepler-539 b revealed a clear modulated TTV signal. We studied this with TRADES, a code able to make a simultaneous fit of RV and mid-transit times and compare the results with simulated data of various multi-planetary configurations. We found that the TTV can be explained through the presence of a 1.2–3.6 $M_{\rm Jup}$ Jovian-like planet c on a very eccentric $(e = 0.43$–$0.61)$ and wider orbit than that of Kepler-539 b, with a period larger than 1000 days. Each of the five solutions that we have presented are related to a planetary system which is stable according to the results of an FMA analysis.

Since the orbit of Kepler-539 c is highly eccentric, then the modulation of the TTV signal of Kepler-539 b can be easily explained. As the distance of planet c from the parent star varies with time, there is a periodic change of the mid-transit time of planet b. In particular, when the planet c is in conjunction with planet b, the gravitational interaction

Table 6: *Left-hand columns*: parameters of Kepler-539 c from the best fit of the *Kepler* mid-transit times and CAFE-RV measurements. The best five solutions obtained with TRADES are shown. *Left-hand columns*: parameters determined from the previous.

Algortihm	M_c ($M_{\rm Jup}$)	P_c (day)	ν_c (°)	e_c	ω_c (°)	χ^2_ν	a (au)	$T_{\rm eq}$ (K)	$TTV_{\rm max}$ (min)
PIKAIA	$3.60^{+0.30}_{-0.23}$	1040^{+30}_{-19}	$33.95^{+0.76}_{-1.02}$	$0.432^{+0.010}_{-0.006}$	$270.67^{+0.05}_{-0.06}$	34.2	2.04 ± 0.04	271 ± 4	31.0 ± 3.6
PSO	$1.27^{+0.05}_{-0.05}$	1705^{+70}_{-49}	$23.13^{+0.84}_{-0.72}$	$0.605^{+0.009}_{-0.005}$	$166.27^{+0.83}_{-0.86}$	39.5	2.84 ± 0.08	230 ± 4	9.3 ± 1.1
PIKAIA	$1.20^{+0.11}_{-0.11}$	945^{+7}_{-6}	$18.00^{+0.57}_{-0.60}$	$0.448^{+0.010}_{-0.010}$	$329.27^{+2.69}_{-2.54}$	57.2	1.91 ± 0.02	280 ± 3	11.8 ± 1.4
PIKAIA	$2.72^{+0.15}_{-0.19}$	1784^{+66}_{-59}	$349.14^{+0.50}_{-0.57}$	$0.563^{+0.010}_{-0.010}$	$296.56^{+2.17}_{-1.70}$	62.9	2.92 ± 0.08	226 ± 4	17.8 ± 2.2
PSO	$2.28^{+0.15}_{-0.16}$	963^{+29}_{-27}	$355.50^{+0.34}_{-0.38}$	$0.457^{+0.009}_{-0.009}$	$343.54^{+1.34}_{-1.05}$	66.6	1.94 ± 0.05	278 ± 4	22.4 ± 2.7

Notes. We used two different algorithm: the PIKAIA algorithm (Charbonneau 1995) and the Particle Swarm Optimization (PSO) algorithm (Tada 2007), respectively. The first five columns refer to the values of the parameters determined from the fitting processes, while the others values have been determined using the previous ones. In particular, δt represents the maximum TTV for the inner planet b.
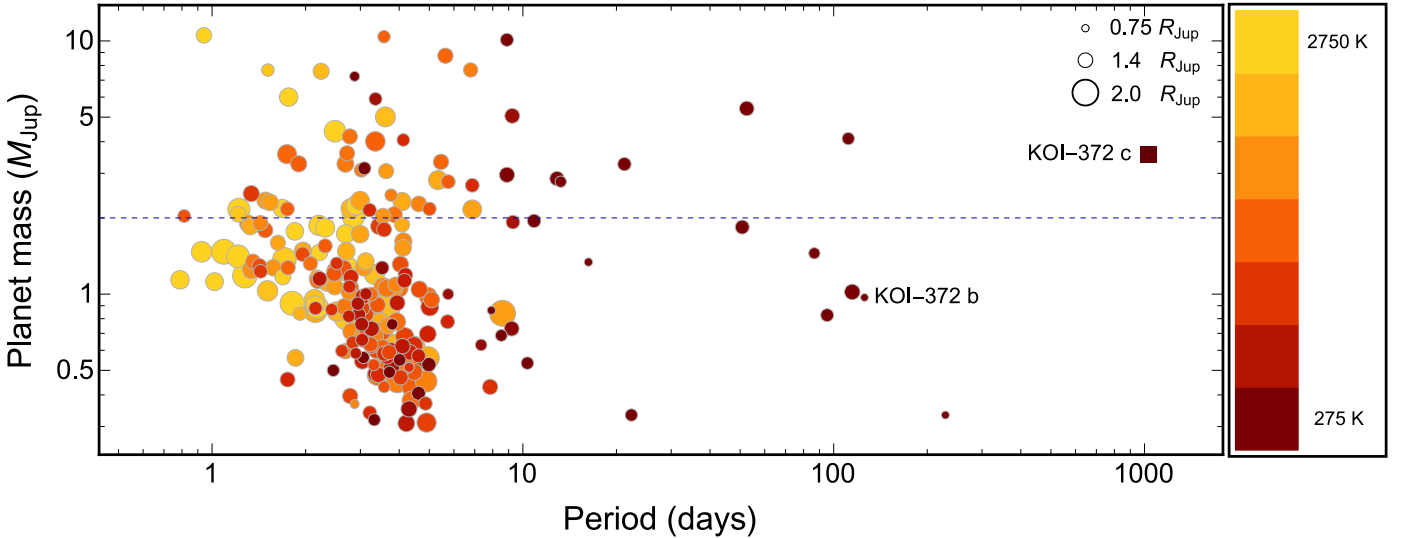
Fig. 9: The *period–planetary mass* diagram for transiting planets in the mass range $0.3\,M_{\rm Jup} < M_p < 11\,M_{\rm Jup}$. The size of each circle is proportional to the corresponding planetary radius, while the colour indicates equilibrium temperature (data taken from TEPCat). The dashed line demarcates the high-mass regime ($M_p > 2M_{\rm Jup}$). The positions of Kepler-539 b and Kepler-539 c are highlighted. Kepler-539 c is marked with a box since we do not know its radius. The error bars have been suppressed for clarity.

between the two planets is maximum and we see a large amplitude of the TTV signal. Then, when planet c moves away, planet b re-circularizes its orbit very slowly and we see the gradual decreasing of the amplitude of its TTV.

Given its relatively young age, the physical parameters of the Kepler-539 planetary system can be very precious for astrophysicists working on theories of planet formation and evolution. If we visualise the known transiting planets, reported in TEPCat[5], in a period–mass diagram, we can see that Kepler-539 b and Kepler-539 c occupy sparsely-populated regions of this plot (here for the mass of Kepler-539 c we have considered the best value found by TRADES).

We also underline that the transits of Kepler-539 b are quite deep (0.8%) and that the host star is relatively bright ($V = 12.5$ mag) and therefore amenable for exoplanet atmosphere studies. The star-planet distance is large enough to consider Kepler-539 b as a non-inflated planet with a low irradiation level. Since there are only a handful of transiting

Jupiter-like planets with a low irradiation level, this planetary system could be a precious target for future studies of exoplanet atmospheres of normal giant gas planets.

Unfortunately, the parameters of Kepler-539 c are not well constrained as they are based on a poorly-sampled TTV (only 12 transit timings). More transits of Kepler-539 b and more precise RV observations with a larger-aperture telescope are required to properly model its TTV signal and accurately determine the existence and the physical properties of Kepler-539 c on a quite solid ground. While there are now several high-resolution spectrographs with RV performance better than CAFE, the observations of new transits of Kepler-539 b are not straightforward with ground-based facilities. The 125.6-day orbital period and the long transit duration (9.31 hr) put serious limitations for the successful of a such long-term monitoring and request a large observational effort with various telescopes located at different Earth's longitudes. Furthermore, the use of different telescopes could compromise the precision of the measurements of T_0 at the end. On the other hand, the observations of new mid-transit times of Kepler-539 b

---

[5] TEPcat (Transiting Extrasolar Planet Catalogue) is available at www.astro.keele.ac.uk/jkt/tepcat/ (Southworth 2011).

can be easily performed by the incoming space telescope CHEOPS. This facility is therefore highly recommended for a new detailed follow-up study of the Kepler-539 planetary system.

References

Aceituno, J., Sãnchez, S. F., Grupp, F., et al. 2013, A&A, 552, A31
Adams, E. R., Ciardi, D. R., Dupree, A. K., et al. 2012, AJ, 144, 42
Alonso, R., Brown, T. M., Torres, G., et al. 2004, ApJ, 613, 153
Alsubai, K. A., Parley, N. R., Bramich, D. M., et al. 2013, AcA, 63, 465
Bakos, G. Á., Noyes, R. W., Kovács, G., et al. 2004, PASP, 116, 266
Bakos, G. Á., Csubry, Z., Penev, K., et al. 2013, PASP, 125, 154
Baranne, A., Queloz, D., Mayor, M., et al. 1996, A&AS, 119, 373
Barge, P., Baglin, A., Auvergne, M., et al. 2008, A&A, 482, L17
Barnes, S. A. 2010, ApJ, 722, 222
Barnes, S. A. & Kim, Y.-C. 2010, ApJ, 721, 675
Barros, S. C. C., Boué, G., Gibson, N. P., et al. 2013, MNRAS, 430, 3032
Blackwell, D. E., Shallis M. J. 1979, MNRAS, 186, 673
Borsato, L., Marzari, F., Nascimbeni, V., et al. 2014, A&A, 571, A38
Borucki, W. J., Koch, D., Basri, G., et al. 2011, ApJ, 736, 19
Charbonneau, P. 1995, ApJS, 101, 309
Ciceri, S., Lillo-Box, J., Southworth, J., et al. 2015, A&A, 573, L5
Doyle, A. P., Davies, G. R., Smalley, B., et al. 2014, MNRAS, 444, 3592
Figueira, P., Faria, J. P., Adibekyan, V. Z, et al. 2016, proceedings of the conference Habitability in the Universe: From the Early Earth to Exoplanets, arXiv:1601.05107
Gandolfi, D., Parviainen, H., Fridlund, M. et al. 2013, A&A, 557, AA74
Gandolfi, D., Parviainen, H., Deeg, H. J., et al. 2015, A&A, 576, A11
Gray R. O., Corbally C. J. 1994, AJ, 107, 742
Grevesse, N., Sauval, A. J. 1998, SSRv, 85, 161
Haswell C. A. 2010, Transiting Exoplanets, Cambridge University Press
Ioannidis, P., Huber, K. F., Schmitt, J. H. M. M. 2016, A&A, 585, A72
Kopparapu, R. K., Ramirez, R., Kasting, J. F., et al. 2013, ApJ, 765, 131
Kopparapu, R. K., Ramirez, R., SchottelKotte, J., et al. 2014, ApJ, 787, L29
Kurucz R. L. 1979, ApJS, 40, 1
Laskar, J., Froeschlé, C., Celletti, A. 1992, Physica D, 56, 253
Lillo-Box, J., Barrado, D., Bouy, H. 2012, A&A, 546, A10
Lillo-Box, J., Barrado, D., Moya, A., et al. 2014a, A&A, 562, A109
Lillo-Box, J., Barrado, D., Henning, Th., et al. 2014b, A&A, 568, L1
Lillo-Box, J., Barrado, D., Bouy, H. 2014c, A&A, 566, A103
Lillo-Box, J., Barrado, D., Mancini, L., et al. 2015a, A&A, 576, A88
Lillo-Box, J., Barrado, D., Santos, N. C., et al. 2015b, A&A, 577, A105
Lind, K., Asplund, M., Barklem, P. S. 2009, A&A, 503, 541
Mancini, L., Southworth, J., Ciceri, S., et al. 2013a, A&A, 551, A11
Mancini, L., Ciceri, S., Chen, G., et al. 2013b, MNRAS, 436, 2
Mancini, L., Southworth, J., Ciceri, S., et al. 2014a, A&A, 562, A126
Mancini, L., Southworth, J., Ciceri, S., et al. 2014b, A&A, 568, A127
Mazeh, T., Holczer, T., Shporer, A. 2015, ApJ, 800, 142

McCullough, P. R., Stys, J. E., Valenti, J. A., et al. 2005, PASP, 117, 783
McQuillan, A., Mazeh, T., Aigrain, S. 2013, ApJ, 775, L11
Oshagh, M., Santos, N. C., Boisse, I., et al. 2013, A&A, 556, A19
Pace, G., Castro, M., Meléndez, J., et al. 2012, A&A, 541, A150
Pepper, J., Pogge, R. W., DePoy, D. L., et al. 2007, PASP, 119, 923
Pollacco, D. L., Skillen, I., Collier Cameron, A., et al. 2006, PASP, 118, 1407
Sestito, P., Randich, S., Pallavicini, R. 2004, A&A, 426, 809
Sestito, P., Randich, S. 2005, A&A, 442, 615
Sing, D. 2010, A&A, 510, A21
Soderblom, D. R., Jones, B. F., Balachandran, S., et al. 1993, AJ, 106, 1059
Southworth, J. 2008, MNRAS, 386, 1644
Southworth, J. 2011, MNRAS, 417, 2166
Southworth, J. 2012, MNRAS, 426, 1291
Southworth, J. 2013, A&A, 557, A119
Straizys, V. & Kuriliene, G. 1981, Ap&SS, 80, 353
Tada, T. 2007, Journal of Japan Society of Hydrology & Water Resources, 20, 450
Takeda, Y., Honda S., Ohnishi, T., et al. 2013, PASJ, 65, 53
Tregloan-Reed, J., Southworth, J., Tappert, C. 2013, MNRAS, 428, 3671
Tregloan-Reed, J., Southworth, J., Burgdorf, M. 2015, MNRAS, 450, 1760
Walkowicz, L. M., & Basri, G. S. 2013a, MNRAS, 436, 1883
Walkowicz, L. M., & Basri, G. S. 2013b, VizieR On-line Data Catalog: J/MNRAS/436/1883

Appendix A: Starspot parameters

In this appendix we report a Table containing the starspot parameters that were determined from the PRISM+GEMC fitting of the transit light curves at cycles -5 and 2, as defined in Sect. 2.1.

Table A.1: Starspot parameters derived from the PRISM+GEMC fitting of the transit light curves at cycles −5 and 2. [a]The longitude of the centre of the spot is defined to be 0° at the centre of the stellar disc and can vary from −90° to 90°. [b]The co-latitude of the centre of the spot is defined to be 0° at the north pole and 180° at the south pole. [c]Angular radius of the starspot (note that an angular radius of 90° covers half of stellar surface). [d]Spot contrast (note that 1.0 equals the brightness of the surrounding photosphere).

Cycle	$\theta(°)$ [a]	$\phi(°)$ [b]	$r_{\mathrm{spot}}(°)$ [c]	ρ_{spot} [d]
−5	-26.18 ± 3.73	28.31 ± 10.14	36.43 ± 6.80	0.69 ± 0.11
2	18.88 ± 11.79	34.27 ± 8.21	18.60 ± 6.46	0.70 ± 0.28

Appendix B: TRADES simulations

In this appendix we report plots based on the results of the
TRADES simulations for modelling the TTV detected in
the transit timings of KOI-327 b. In particular, the figures
show RV plots (bottom panels) and O–C diagrams from lin-
ear ephemeris for planet Kepler-539 b (top panels). In both
cases, the observed data are compared with those obtained
from the simulations (see Sect. 4) The figures are ordered
as in Table 6. Figures 1, 3 and 4 were obtained by using
the PIKAIA algorithm (Charbonneau 1995), while figures
2 and 5 with the Particle Swarm Optimization (PSO) algo-
rithm (Tada 2007).
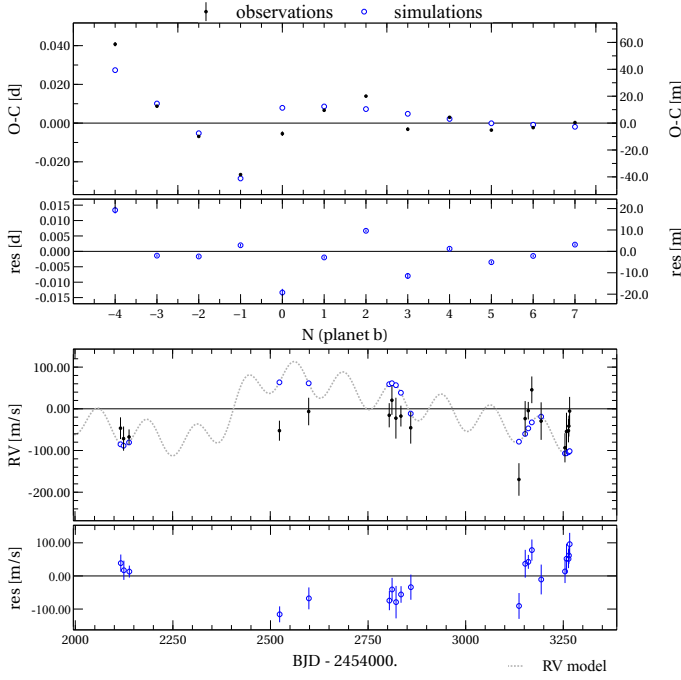
Fig. B.1: O–C diagram (with residuals) from linear
ephemeris for planet Kepler-539 b (top panel); observations
plotted as black points (with error bars), simulations plot-
ted as open blue circles. Bottom panel shows the RV ob-
servations as solid black circles, simulations at the same
BJD(UTC) as open blue circles, and the dotted gray line
is the RV model for the whole simulation. This the best
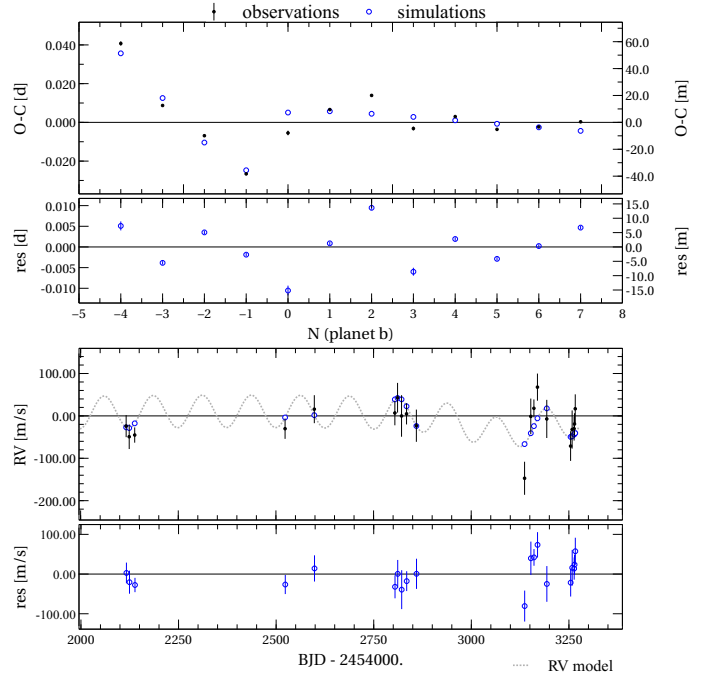solution found by TRADES.

Fig. B.2: Same as for Fig B.1, but showing the 2nd best so-
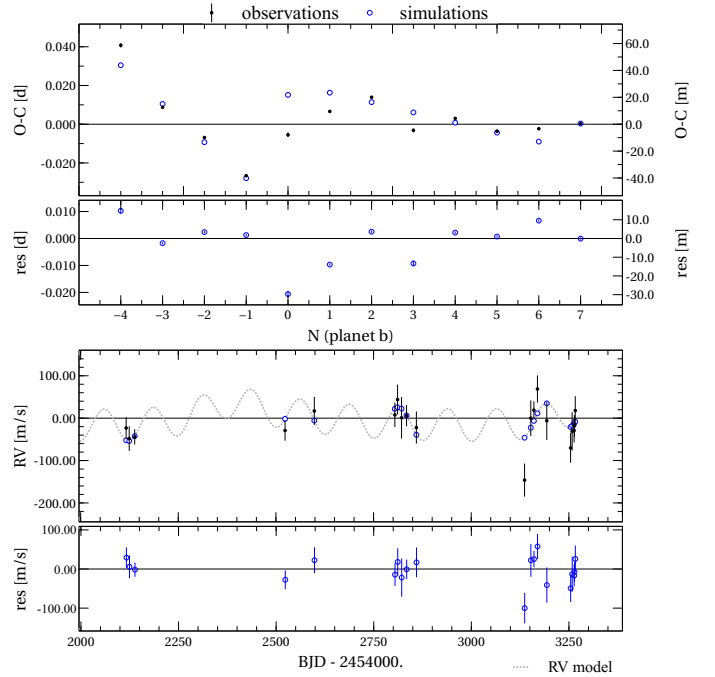lution found by TRADES.

Fig. B.3: Same as for Fig B.1, but showing the 3rd best so-
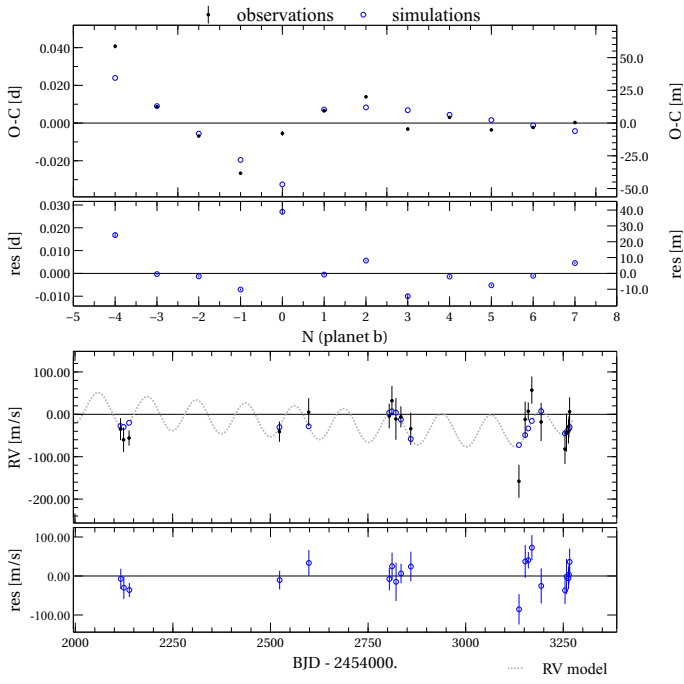lution found by TRADES.

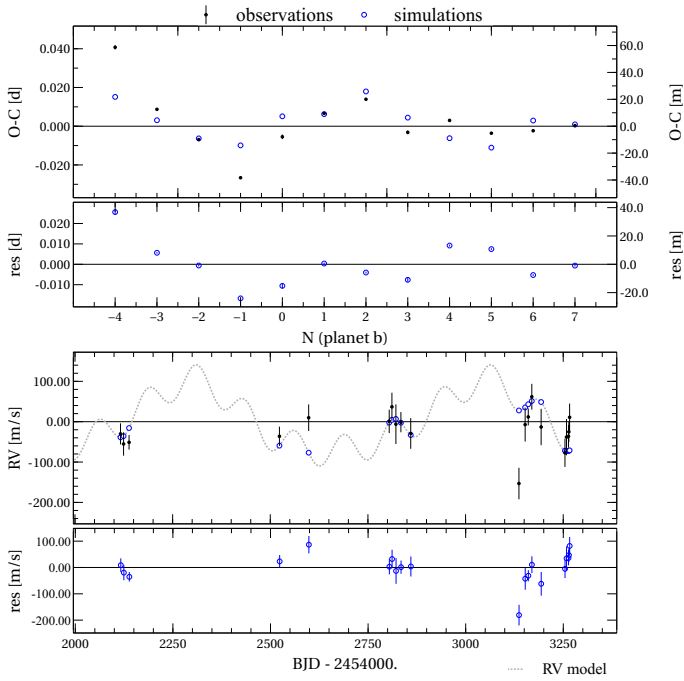Fig. B.4: Same as for Fig B.1, but showing the 4th best solution found by TRADES.

Fig. B.5: Same as for Fig B.1, but showing the 5th best solution found by TRADES.